SEM study of dolomite microcrystals in Grenville marble

Ralph Kretz

Department of Geology, University of Ottawa, Ottawa K1N 6N5, Canada

Abstract

Microcrystals of dolomite within crystals of calcite in high-grade Grenville marble occur as oriented plates, 20 μm to 1 mm across, as parallel or radiating rods, 100 to 400 μm long; and as small, commonly interconnected particles, 1 to a few micrometers across. The microcrystals evidently separated from magnesian calcite during slow cooling from a peak metamorphic temperature of about 700 °C.

The Mg content of "calcite" (calcite + very small dolomite particles) decreases as dolomite plates and rods are approached, and the concentration vs. distance curves are viewed as stranded diffusion profiles. Plates and rods contain five times as much Fe and half as much Sr as the surrounding "calcite," which shows that these elements were also involved in the separation process.

Some small dolomite particles occur as rhombohedra [rarely truncated by (0001)], coaxial with the enclosing calcite. Calculated dislocation densities on the interface planes at seven points on the presumed cooling path are lower on (0001) than on (10$\bar{1}$1) (e.g., 4.0 × 10^{11} and 5.2 × 10^{11} cm^{-2}, respectively, at 500 °C and 5 kbar). Conversely, the chemical component of interfacial energy may be lower on (10$\bar{1}$1) (the cleavage plane) than on (0001). Hence both forms may be present in the equilibrium shape of a dolomite particle embedded in calcite.

Three successive stages in the separation of dolomite from magnesian calcite are proposed, reflecting a progressive increase in nucleation rate and decrease in diffusion rate: (1) exsolution of dolomite to grain boundaries, (2) nucleation within crystals of calcite and subsequent growth to form plates and rods, and (3) precipitation of very small particles. During stage (2), dolomite plates (representing a departure from the equilibrium shape) were produced by rapid advance of rhombohedral relative to basal interfaces, and segmented rods were produced by the dendritelike propagation of rhombohedra from side corners of preceding rhombohedra.

Introduction

Oriented plates and rods of dolomite within crystals of calcite are frequently observed in medium- to high-grade marble and in carbonatite. An X-ray study of such intergrowths led Goldsmith (1960) to conclude that the dolomite microcrystals exsolved from magnesian calcite during slow cooling. Numerous questions remain, however, concerning the role of interfacial energy and reaction mechanisms in determining the properties of the dolomite particles.

Information on the morphology of dolomite microcrystals is readily obtained by examining etched grains of calcite with a scanning electron microscope (Puhan, 1984). This method, when applied to specimens of marble from the Grenville province revealed a great diversity of dolomite particles, including plates, rods, rhombohedra, and others of more irregular shape. These features are here illustrated and described, together with chemical analyses of dolomite plates and rods and the enclosing calcite.

Dolomite particles in the study specimens evidently separated from magnesian calcite during slow cooling of the Grenville terrane from about 700 °C, and it is assumed that separation occurred by a solid-state exsolution process. The presence of "stranded diffusion profiles" adjacent to some rods and plates is presented as evidence in support of this assumption.

In examining the microstructures, questions immediately arise regarding the cause for the great diversity that was observed. Why, for example, were plates produced in one calcite grain and rods in an adjacent one? Although the answers to such questions are not readily found, some interpretations are presented concerning the role of interfacial energy, volume changes, and various processes (diffusion, nucleation, crystal growth) in controlling the exsolution reaction.

Preliminary considerations

Previous study

Coomaraswamy (1902) presented illustrations of oriented plates and rods of dolomite in crystals of calcite from high-grade marble of Sri Lanka. Joplin (1935) observed similar features in contact marbles of New South
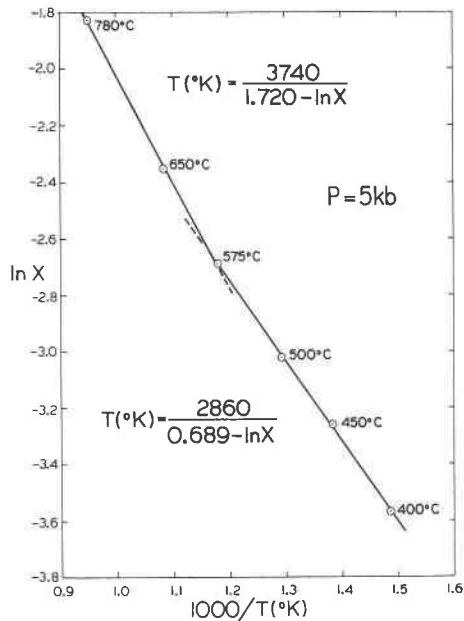
Fig. 1. The calcite limb of the 5-kbar calcite-dolomite solvus of Goldsmith and Newton (1969) on a ln X vs. T^{-1} plot, where X is mole fraction $MgCO_3$ in calcite and T is absolute temperature. Data points represent the mean of two or more runs, as follows: 400 °C (2 runs), 450 °C (4 runs), 500 °C (3 runs), 575 °C (3 runs), 650 °C (14 runs; one extreme omitted), 780 °C (11 runs; two extremes omitted). Uncertainty (±2 standard deviations) in ln X at 780 and 650 °C is approximately equal to the diameter of the circles shown; at 575, 650, and 450 °C, equal to twice the circle diameter; and at 400 °C, equal to three times the circle diameter.

Wales and was evidently first to suggest that the microstructures were the result of exsolution.

Although dolomite microcrystals in marble and carbonatite have been reported from numerous localities, only a few detailed investigations of these crystals have been carried out. Goldsmith (1960) confirmed by use of X-rays that both visible and submicroscopic crystals of dolomite occur in calcite from various localities and that the crystallographic orientation of the crystals is commonly parallel to that of the host calcite. He also induced dolomite to exsolve from a high-Mg (metastable) calcite by heating it for 7 d at 500 °C and 54-bars CO_2 pressure. The morphology of the exsolved phase was not determined.

Carpenter (1967) described clusters of subparallel rods of dolomite in crystals of calcite in high-grade marble at Crestmore, California, and noted that the crystallographic orientation of the rods is not always parallel to that of the host calcite. Puustinen (1974) observed rods, lamellae (up to 10 mm in greatest dimension), and irregular dolomite inclusions in calcite of the Siilinjärvi carbonatite of Finland, where small grains of dolomite also occur on calcite grain boundaries. Puhan (1984) noted that in certain marbles from Namibia, dolomite microcrystals occur dominantly as radiating rods. SEM images showed that
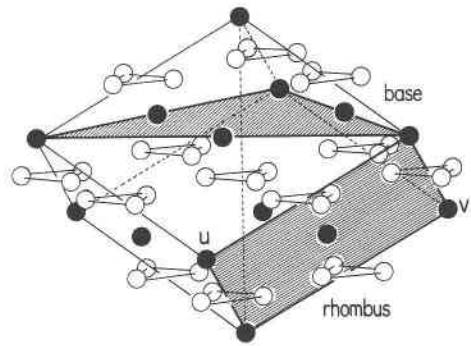

Fig. 2. The calcite structure, showing planes parallel to the cleavage rhombohedron (from Evans, 1966); u to v is the long diagonal.

some rods are segmented, i.e., they consist of several stacked rhombohedra. Nesbitt and Essene (1982) noted that in a portion of the Blue Ridge province, dolomite microcrystals in medium-grade marble occur principally as random elongate crystals up to 85 μm long, concentrated in the central regions of calcite grains.

The chemical composition of calcite grains that enclose microcrystals of dolomite has been determined by Goldsmith et al. (1955), Goldsmith (1960), Sheppard and Schwarcz (1970), Ioffe et al. (1973), Rice (1977), Garde (1977), Gittins (1979), and others. The general finding is that the calcite varies greatly in Mg content, both from one grain to another in a small volume of rock and from one spot to another in a single crystal. Long and Agrell (1965) and Puustinen (1974) analyzed host calcite and dolomite lamellae and found the latter enriched in Fe, which indicates that minor elements are also involved in the separation process.

The proposal that dolomite rods and plates had separated from magnesian calcite during cooling was supported by the experimental results of Harker and Tuttle (1955), which showed that the maximum solubility of $MgCO_3$ increases with increasing temperature, to 12 mol% at 700 °C. Hence, up to 24 mol% dolomite could conceivably separate from calcite as temperature decreased from 700 °C (high-grade metamorphic conditions) to Earth-surface temperatures.

Phase relations

Phase relations in the system $CaCO_3$-$MgCO_3$ were investigated by Harker and Tuttle (1955), Goldsmith and Heard (1961), and Goldsmith and Newton (1969). Of special interest is the appearance of the phase dolomite $Ca_{0.5}Mg_{0.5}CO_3$ of nearly fixed composition and the presence of a solvus that defines the $MgCO_3$ content of calcite in equilibrium with dolomite.

The calcite limb of the Goldsmith-Newton solvus at 5-kbar pressure and 780 to 400 °C is replotted in Figure 1, which shows that the solvus in this range of temperature may be represented by two linear equations:
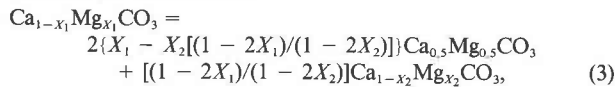
For T = 400 to 575 °C, X = 0.0283 to 0.0683,
$$T = 2860/(0.689 - \ln X), \qquad (1)$$
and for T = 575 to 780 °C, X = 0.0683 to 0.161,
$$T = 3740/(1.720 - \ln X), \qquad (2)$$

where X is the mole fraction of $MgCO_3$ in calcite and T in the equations is in kelvins. The first of these equations was used to extrapolate the limb to 100 °C.

Goldsmith and Newton (1969) determined that the effect of pressure on the solvus is small; a 1-kbar increase in pressure at 450–780 °C produces an increase in the solubility of $MgCO_3$ in calcite that lies within the range of 0.09 to 0.15 mol%.

The phase relations show that calcite in dolomite-bearing marble at 700 °C and about 7-kbar pressure (corresponding to a depth of 20 km) should contain 12 mol% of $MgCO_3$ in solid solution. Provided equilibrium is maintained during uplift, cooling, and decompression, the Mg should separate in the form of dolomite. Mass-balance considerations lead to the following equation for this reaction:

$$Ca_{1-X_1}Mg_{X_1}CO_3 =$$
$$2\{X_1 - X_2[(1 - 2X_1)/(1 - 2X_2)]\}Ca_{0.5}Mg_{0.5}CO_3$$
$$+ [(1 - 2X_1)/(1 - 2X_2)]Ca_{1-X_2}Mg_{X_2}CO_3, \quad (3)$$

which is equivalent to Equation 3 of Graf and Goldsmith (1955). Here X_1 and X_2 are the initial and final mole fractions of $MgCO_3$ in calcite. If the reaction proceeds to completion ($X_2 = 0$), the equation is

$$Ca_{1-X_1}Mg_{X_1}CO_3 = 2X_1Ca_{0.5}Mg_{0.5}CO_3 + (1 - 2X_1)CaCO_3. \quad (4)$$

Equation 3 will be used below to estimate the volume change accompanying the exsolution reaction.

Crystal structure

The structures of magnesian calcite and dolomite differ in several properties (Reeder, 1983). Representative cell dimensions of calcite containing 10 mol% $MgCO_3$ are $a = 4.941$, $c = 16.864$ Å (Althoff, 1977), and those of dolomite are $a = 4.807$, $c = 16.002$ Å (Reeder and Markgraf, 1986). The cation-O_6 octahedra in calcite are more distorted than in dolomite and are rotated slightly relative to their position in dolomite. In calcite the C and three adjacent oxygen ions are coplanar, whereas in dolomite the C atoms lie slightly out of the oxygen plane.

The above comparison suggests that a calcite-dolomite interface should represent a discontinuity, even if crystal axes are coincident. Cell dimensions are sufficiently similar to suggest that the interface may be semicoherent as proposed by Grover and Kubanek (1983).

Of special importance for the present study are the $(10\bar{1}1)$ cleavage planes for these are readily located in thin sections and SEM images and form convenient planes of reference. The term *rhombohedron*, as used below, refers to the cleavage rhombohedron, as shown in Figure 2.

OCCURRENCE AND COOLING PATH

Study specimens were collected from a portion of the Grenville province (Canadian Precambrian shield) north of the Ottawa River, where calcite-dolomite marble occurs abundantly, interlayered with gneisses, quartzite, and amphibolite (Kretz, 1980). The grade is upper-amphibolite to lower-granulite facies, and temperature-pressure estimates for the peak of metamorphism are 650–700 °C, 5–7 kbar (Kretz, 1980 and unpub. data; Perkins et al., 1982). A linear P-T path, extending from 700 °C and 7 kbar to 100 °C and 1 kbar, is assumed.

The average rate of cooling is estimated at 1 °C/m.y., based on the assumption that the peak of metamorphism coincided with the Grenville orogeny (dated at 1.1 Ga;


Fig. 3. View of microstructure in specimen 5, showing dolomite rods (i) enclosed by optically continuous calcite (I), dolomite plates (h) enclosed by optically continuous calcite (H) and optically discontinuous calcite (H'), and discrete grains of dolomite (g) some of which may be of exsolution origin. Ap = apatite.

Easton, 1986) and that the marble units reached the surface about 0.50 Ga, shortly before they were covered by Late Cambrian sediments (Wilson, 1964). ^{40}Ar-^{39}Ar data for the Bark Lake Gabbro, 120 km to the southwest, indicate a sigmoidal time-temperature path, with cooling rates in a portion of the path (from 1.0 to 0.95 Ga) as high as 6 °C/m.y. (Berger and York, 1981).

MICROSTRUCTURE

Dolomite microcrystals in calcite are most easily detected when a cut rock surface is etched with dilute HCl, then stained with alizarin-red S solution, and examined with a binocular microscope. Supplementary examination in thin section enables one to determine whether the c axes of dolomite and calcite are parallel.

Within a group of 120 specimens of marble, which formed the subject of a previous study (Kretz, 1980), 30 specimens contain optically visible plates and rods similar to those shown in Figure 3. They are especially conspicuous in forsterite + calcite + dolomite marble where, because of the reaction

tremolite + 11 dolomite = 8 forsterite + 13 calcite
$+ 9CO_2 + H_2O$,
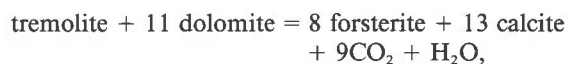
as defined by Skippen (1974) and Metz (1976), metamorphic temperatures may have been slightly higher than in tremolite + dolomite + calcite marble, resulting in a higher proportion of $MgCO_3$ in calcite.

Within the group of 30 specimens referred to above, rods are more common than plates, but plates tend to be
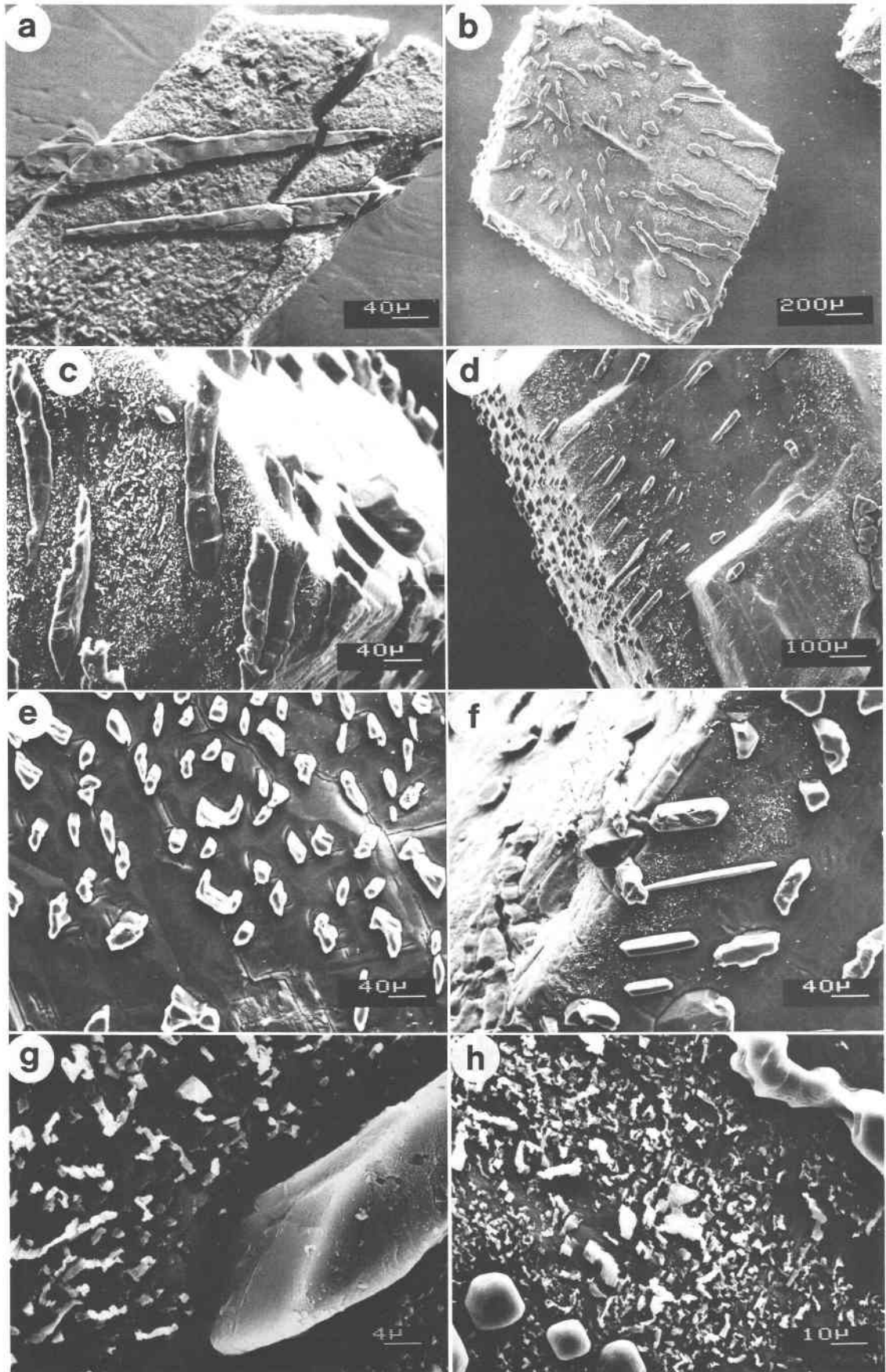
Fig. 4. SEM micrographs of dolomite microcrystals (in relief) in etched calcite. See text for description.
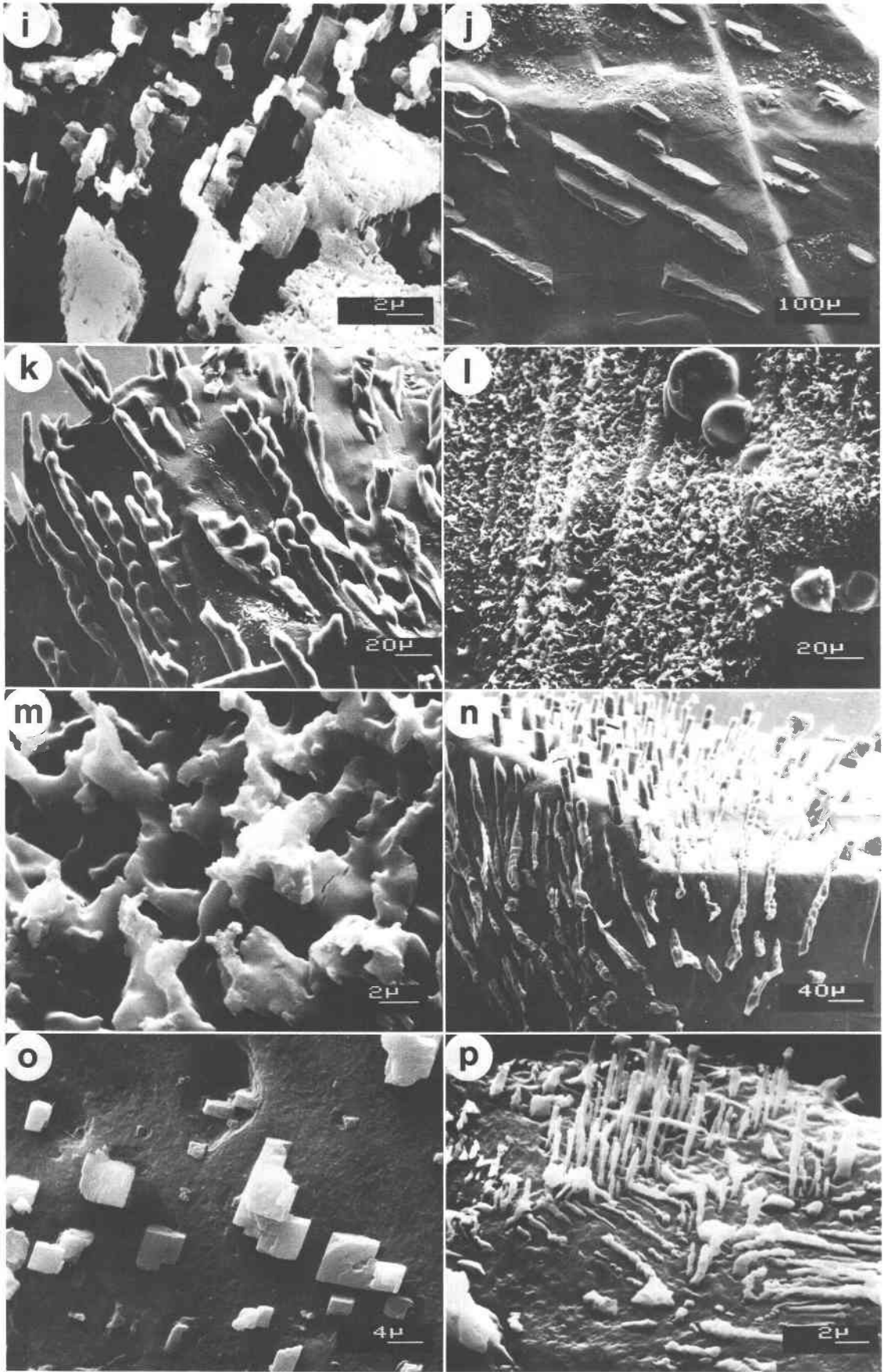
Fig. 4—*Continued.*

larger, up to 3 mm in greatest dimension. Most plates lie parallel to the long diagonal of the cleavage rhombus, whereas rods commonly radiate from the center of a grain. The optic axes of most plates and rods are parallel to those of the host calcite, but exceptions occur, as shown in Figure 3. Here dolomite plates (h) are enclosed by optically parallel calcite (H) and also by calcite (H′) that has a different orientation and is presumably recrystallized calcite. Also shown in Figure 3 are oriented rods (i) optically parallel to the enclosing calcite (I), and (on calcite grain boundaries), small grains of dolomite (g), which may represent additional exsolved dolomite.

Crystals of calcite and dolomite that are optically parallel are presumably crystallographically parallel, as was the case for two specimens from the area investigated by Goldsmith (1960).

Five specimens of marble, each about 1 cm³ in volume, were selected for detailed examination. They contain 70 to 90% calcite, 2 to 10% dolomite as discrete grains (similar in size to those of calcite), and small amounts of other minerals (forsterite, diopside, tremolite, phlogopite, and humite group minerals). The specimens were crushed and sieved, and a few hundred particles 1 mm in diameter (many forming cleavage rhombohedra) were etched for 6 s in very dilute HCl and stained lightly with alizarin-red S solution. Several fragments from each specimen were then selected, mounted, coated with Au, and examined with a Semco SEM instrument.

Identification of the microcrystals as dolomite is based on single-crystal X-ray techniques (two specimens examined by Goldsmith, 1960), semiquantitative energy-dispersive analysis, and microprobe analysis.

In specimen 1 (Fig. 4a), dolomite plates are more abundant than rods. The plates lie parallel to the long diagonal of the rhombus and hence normal to c of the calcite host.

In specimen 2, dolomite microcrystals occur principally as rods and fine particles. Figure 4b shows rods radiating from a point within a calcite crystal, but with a tendency for the rods to lie within a rhombohedral plane. The emergence of rods on three other planes is visible. In some calcite crystals, the rods are parallel rather than radiating; this is shown in Figure 4c, where they lie parallel to the long diagonal of one rhombus of calcite. Very small particles of dolomite are also visible.

Figure 4d shows a swarm of rods lying at a small angle to one of the three rhombohedral planes, and at a small angle to the line of intersection of two planes. Fine particles of dolomite are very unevenly distributed.

A variation in the cross-sectional shape of some rods is shown in Figure 4e. Measurements on the spacing of these rods (the nearest-neighbor method, Kretz, 1969) confirm that the distribution is anticlustered.

Rods, plates, and fine particles in another crystal of calcite from specimen 2 are shown in Figure 4f. The ratio of plate width to plate thickness varies greatly (hence not all of the dolomite plates represent the equilibrium shape), but the terminations of all plates appear to be rhombohedral faces.

Zones of diminishing abundance of small dolomite particles and of enhanced etching of calcite occur about some dolomite rods (Fig. 4g); microprobe analyses of these zones are presented below.

Figure 4h shows an irregular platelike microcrystal of dolomite (top right) and some small rhombohedra with rounded edges (bottom left) and reveals the nature of some of the finer dolomite particles. A closer view (Fig. 4i) shows that these particles are partially bounded by rhombohedral planes and form an interconnected network.

Dolomite microcrystals in specimen 3 occur as plates and fine particles. Plates vary greatly in size, as shown in Figure 4j where they lie normal to c of host calcite and are distributed at random. In places, cleavage planes in plates are observed to lie parallel to those in the host, thus confirming that a and c axes of dolomite coincide with those of calcite. Rare views of plates from "above" show them to be nearly circular in plan.

In specimen 4, rods are abundant and are distinctly segmented, as shown in Figure 4k. Each segment appears to be a rhombohedron, and the rods may be viewed as a group of connected rhombohedra, with an infilling of corners and rounding of edges by additional dolomite precipitation. Similar rods were previously described by Puhan (1984).

Disk-shaped plates and a network of very fine dolomite are shown in Figure 4l; the network is shown in greater detail in Figure 4m. Rhombohedral planes are not as well developed as in specimen 3 (Fig. 4i).

In specimen 5 (also illustrated in Fig. 3), both rods and plates are present, and a group of segmented rods is shown in Figure 4n. Several grains of calcite, apparently free of rods and plates when viewed with a light microscope, were found to contain about 12 vol% of very small dolomite crystals. These occur mainly as irregular, near-equidimensional particles, 1–10 μm in diameter, but locally occur as well-formed rhombohedra (Fig. 4o) with faces parallel to rhombohedral planes in the calcite host. Rarely (bottom right of Fig. 4o), small basal (0001) faces are present. Clusters of very small rods and plates (Fig. 4p) are locally present; the rods, which are also segmented, are only 0.5 μm in diameter.

In summary, dolomite microcrystals in the study material occur as (1) plates, 20 μm to 1 mm (occasionally larger) across, oriented normal to c of the host calcite, and with square or rhombohedral terminations; (2) smooth and segmented rods, 100 to 400 μm long (occasionally much smaller), that commonly occur as radiating or parallel clusters lying within a rhombohedral plane of the host calcite; (3) bodies of more irregular shape that may be viewed as imperfectly formed plates or rods; and (4) small particles, 1 to a few micrometers in maximum dimension, commonly interconnected, and ranging in shape from irregular to well-formed rhombohedra.

CHEMICAL COMPOSITION

X-ray determinative curves of Goldsmith et al. (1955) were used to estimate the Mg content of 14 samples of

TABLE 1. Microprobe analyses (wt%) of dolomite rods and plates and enclosing "calcite"

	Specimen 2			Specimen 3		
	Dolomite rods	Adjacent "calcite"	Distant† "calcite"	Dolomite plates	Adjacent "calcite"	Distant‡ "calcite"
CaO	30.3(0.3)	54.3(0.2)	54.6(0.5)	30.5(0.6)	53.9(0.4)	54.0(0.3)
MgO	21.2(0.3)	1.71(0.05)	1.86(0.09)	21.2(0.5)	1.92(0.08)	2.06(0.07)
FeO*	0.46(0.04)	0.082(0.04)	0.092(0.04)	0.57(0.04)	0.14(0.03)	0.10(0.01)
SrO	0.07(0.02)	0.14(0.02)	0.12(0.02)	0.04(0.02)	0.06(0.03)	0.08(0.02)
CO_2**	47.0	44.6	45.0	47.4	44.5	44.7
Sum	99.0	100.8	101.7	99.7	100.5	100.9
n	10	5	5	5	6	6

Note: Obtained by use of a CAMECA CAMEBAX Micro System at McGill University, and their MBXCOR Micro software package. Operating conditions: accelerating voltage 15.0 kV, current 10 nA, beam width 5 μm, counting time 20 s. Natural minerals (dolomite, ankerite, strontianite) were employed as standards. "Calcite" refers to average of calcite and very small dolomite particles, as seen in Fig. 4c (specimen 2) and 4j (specimen 3). Values in parentheses are estimates of local variability (1 standard deviation) based on *n* spot determinations.
* Total Fe expressed as FeO.
** Calculation, based on molar CO_2:(Ca,Mg,Fe,Sr)O = 1:1.
† 15 μm from rods.
‡ 10 to 50 μm from plates.

calcite from calcite-dolomite marble of the study area. Two additional samples were analyzed by Goldsmith (1960). The results reveal a broad variation in composition, ranging from nearly pure $CaCO_3$ to 7.6 mol% $MgCO_3$, the latter value corresponding to a temperature of 600 °C. Provided that the calcite crystals were saturated with $MgCO_3$ at the peak of metamorphism, the observed variation in composition indicates a corresponding variation, from place to place, in the progress of the reaction by which dolomite separated from calcite.

In an earlier study (Kretz, 1980), grains of calcite (together with the enclosed dolomite microcrystals) were separated from 24 specimens of calcite-dolomite marble from the study area and analyzed by atomic absorption spectroscopy. The grains contain low levels of FeO, MnO, and SrO (<0.5 wt% for each) and show a variation in $MgCO_3$ content from 2.4 to 8.6 mol%. These data indicate that some $MgCO_3$ was transported to grain boundaries, where it crystallized as secondary dolomite. It is difficult to distinguish this dolomite from primary dolomite, but small grains located at calcite-calcite grain boundaries, in optical continuity with one of the adjoining calcite grains (e.g., crystal g at top center of Fig. 3), may represent exsolved dolomite.

Microprobe analyses (Ca, Mg, Fe, Sr) were obtained for dolomite rods and the enclosing "calcite" in specimen 2 and for dolomite plates and the enclosing "calcite" in specimen 3 (Table 1). Very small and unevenly distributed particles of dolomite were observed by SEM in both specimens (Figs. 4c and 4j); consequently, each "calcite" analysis (produced by an electron beam of 5-μm diameter) probably represents an average of calcite plus some dolomite inclusions.

Dolomite rods and plates contain more Fe and less Sr than is present in the enclosing "calcite"; the distribution coefficients are 4.7 and 0.50, respectively. These numbers are comparable to estimated distribution coefficients for the peak of metamorphism (e.g., the ratio of the atomic fraction of Fe in primary dolomite to the atomic fraction

of Fe in calcite plus *all* dolomite inclusions) of 3.4 and 0.40, respectively (Kretz, 1980). Hence, Fe and Sr as well as Mg participated in the process that separated dolomite from magnesian calcite, in agreement with results previously obtained by Long and Agrell (1965) and Puustinen (1974).

In both specimens (2 and 3), the "calcite" near dolomite rods and plates was found to be slightly poorer in Mg than "calcite" 10 to 50 μm away. Although the differences are small, application of the *t*-test (Hoel, 1964) to five adjacent vs. distant pairs of "calcite" analyses at five different rods in specimen 2 confirms that the differences are real. Average values are listed in Table 1, row 2. The lower Mg content near the rods evidently reflects a lower concentration of small dolomite particles (Fig. 4g).

A microprobe traverse across one of the rods in specimen 2 is shown in Figure 5. The Mg/(Ca + Mg) vs. distance profile may be a stranded diffusion profile, similar to Ni profiles in kamacite near taenite lamellae (Agrell et al., 1963) and Ca profiles in orthopyroxene near Ca pyroxene lamellae (Lorimer and Champness, 1973). A preliminary fit to the data is provided by the following diffusion equation (derived by Crank, 1975), which applies under greatly simplified boundary conditions (i.e., radial diffusion toward a very long cylinder, steady-state conditions, constant diffusion coefficient):

$$C = [C_1\ln(b/r) + C_2\ln(r/a)]/\ln(b/a).$$

In this equation, C denotes Mg concentration [expressed as atomic percent Mg/(Ca + Mg)]; r is distance radially outward from the axis of the cylinder; C_1 is concentration at the interface (where $r = a = 15$ μm), taken as 4.1; and C_2 is concentration away from the cylinder (where $r = b = 100$ μm), taken as 5.4. These results are supportive of the proposal that the dolomite rods and plates are the result of an exsolution process. Moreover, they suggest that the process was diffusion-controlled.

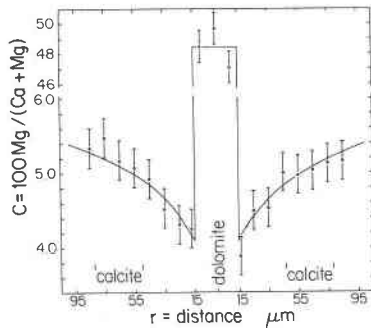Mass-balance calculations of the Mg and Ca transfer

Fig. 5. Microprobe traverse across a dolomite rod and adjacent "calcite" in specimen 2, showing variation in atomic percent Mg/(Ca + Mg) with distance (r). Error bars (± 2 standard deviations) were calculated from estimates of relative standard deviation (counting error) of 0.01 and 0.03 for CaO and MgO determinations in "calcite" and 0.01 and 0.02 for CaO and MgO determinations in dolomite, and by propagating these errors to the atomic ratio Mg/(Ca + Mg). The curves follow the diffusion equation $C = [4.1 \ln(100/r) + 5.4 \ln(r/15)]/1.9$.

implied by Figure 5 show that the Mg-depleted zones could have provided all of the Mg required to construct the central dolomite rod, provided the zone is expanded to a distance of 180 μm from the rod, and the initial Mg/(Ca + Mg) ratio of calcite was 0.06.

If the profile in Figure 5 is indeed a diffusion profile, then it follows that the small dolomite particles shown in Figure 4g postdate the rods and crystallized most abundantly away from them, where the Mg content of calcite was highest. The atomic fractions of Mg in "calcite" near the rods in specimen 2 (i.e., 0.042) and near the plates in specimen 3 (i.e., 0.047) provide estimates of the temperatures of rod and plate formation of 470 and 490 °C, respectively (Fig. 1, Eq. 1). Upon further cooling, rod and plate crystallization evidently declined, and the crystallization of small particles was initiated.

CALCITE-DOLOMITE INTERFACE PLANES

It is generally assumed that the shape and orientation of exsolution lamellae are largely determined by the specific interfacial free energy of the lamellae-host interface planes and that in some cases the total interfacial free energy of a microcrystal is minimized to produce an equilibrium shape. The interfacial free energy per unit area

consists of a chemical part, which dominates if the interfaces are incoherent, and a structural part, which dominates if the interfaces are coherent. Detailed calculations of lattice misfit and coherency strain, such as those performed by Bollmann and Nissen (1968), Robinson et al. (1977), Willaime and Brown (1974), and Fleet (1982), are not attempted here. Rather, the nature of certain dolomite-calcite interfaces and the equilibrium shape of dolomite are examined in qualitative terms, employing the terminology used in metallurgy, as reviewed by Porter and Easterling (1981).

It is evident from Figure 4 that although a great variation exists in the orientation of interface planes, basal (0001) and rhombohedral ($10\bar{1}1$) planes, adjoining coaxial crystals of calcite and dolomite occur commonly. These planes and another, ($10\bar{1}0$), which is not common, are now examined with regard to lattice misfit, dislocation density, and relative interfacial energy.

A modified version of the O-lattice theory of Bollmann (1970) was applied by Grover and Kubanek (1983) to show that the best atomic fit of a crystal of dolomite and one of pure calcite is obtained when **a** and **c** axes of the two crystals are coincident and when the interface plane is (0001). The interface was assumed to be semicoherent. These conclusions will likely apply at higher temperatures, where an increase in the Mg content of calcite would cause the cell dimensions of calcite and dolomite to converge.

Estimates of lattice misfit on (0001) and other interface planes at elevated temperature and pressure may be obtained by use of the following data: (1) the $MgCO_3$ content of calcite as a function of temperature (Eqs. 1 and 2), (2) the cell dimensions of magnesian calcite (Bischoff et al., 1983) and dolomite (Reeder and Markgraf, 1986), (3) the thermal expansion of calcite (Markgraf and Reeder, 1985) applied to magnesian calcite, (4) the thermal expansion of dolomite (Reeder and Markgraf, 1986), (5) the compressibility of calcite (Birch, 1966) applied to magnesian calcite, and (6) the compressibility of dolomite, assumed equal to that of calcite because of the similarity of volume compressibility (Birch, 1966). The resulting cell dimensions for magnesian calcite and dolomite at seven points on the adopted temperature-pressure-composition path are presented in Table 2 and Figure 6. The 95% confidence limits to these estimates are approximately ± 0.003 for a and ± 0.01 for c.

TABLE 2. Calculated cell dimensions and volume of magnesian calcite and dolomite

T (°C)	P (kbar)	X^*	Magnesian calcite			Dolomite		
			a (Å)	c (Å)	V (Å³)	a (Å)	c (Å)	V (Å³)
700	7	0.119	4.918	17.091	358.0	4.818	16.188	325.4
600	6	0.077	4.937	17.114	361.2	4.815	16.149	324.2
500	5	0.049	4.952	17.121	363.6	4.812	16.115	323.1
400	4	0.028	4.964	17.115	365.2	4.811	16.080	322.3
300	3	0.0135	4.974	17.106	366.5	4.809	16.056	321.6
200	2	0.0047	4.982	17.090	367.3	4.808	16.029	320.9
100	1	0.0009	4.987	17.072	367.7	4.807	16.012	320.4

* X = mole fraction $MgCO_3$ in calcite.

From 700 °C, 7 kbar to 100 °C, 1 kbar, the c and a dimensions of dolomite decrease progressively, reflecting a dominance of thermal expansion over compressibility. Changes in magnesian calcite are more complex. A progressive increase in a results from a decrease in $MgCO_3$ content and from (anomalous) expansion on cooling. In the same interval, c expands with decreasing $MgCO_3$ content and contracts as a result of cooling, causing it to pass through a maximum (Fig. 6).

The spacing of Ca and Mg cations along lines parallel to crystallographic a, c, and the edges of rhombohedral planes (denoted ϵ) for magnesian calcite and dolomite are compared in terms of a misfit parameter defined as

$$\delta = (d_{calcite} - d_{dolomite})/d_{dolomite},$$

where d is cation spacing in any dimensional units. The value of δ decreases with increasing temperature, as expected, and misfit along a is considerably less than along c (Table 3).

These results permit one to estimate dislocation density in different directions and hence on different interface planes. The dislocation spacing (D) along a, for example, is

$$D_a = a_{calcite}/\delta_a.$$

Dislocation density on interface planes (0001), (10$\bar{1}$0), and (10$\bar{1}$1) obtained by this procedure are also listed in Table 3. For example, at 100 °C, 1 kbar the calculated dislocation density on (0001) is 6.5×10^{11} cm^{-2}, which may be compared with a value of 6.4×10^{11} cm^{-2} at standard temperature and pressure obtained by Grover and Kubanek (1983).

The specific interfacial free energy (γ) associated with (0001) or other interfaces consists of a structural part (γ_{st} that is proportional to coherency strain and a chemical part (γ_{ch}) that includes an entropy term and is sensitive to temperature. Thus,

$$\gamma = \gamma_{st} + \gamma_{ch}$$

(Porter and Easterling, 1981). The misfit on (0001) and (10$\bar{1}$1), estimated above, is sufficiently small to suppose that γ_{st} is proportional to dislocation density, and hence from Table 3, in the range of 700 °C, 7 kbar to 100 °C, 1 kbar,

$$\gamma_{st,(0001)}, < \gamma_{st,(10\bar{1}1)}.$$

Relative values of γ_{ch} are not known, but γ_{ch} for the rhombohedral interface is expected to be especially low, given the excellent cleavage on this plane and given the calculation of Stranski (1949) to show that the equilibrium shape for calcite in a $CaCO_3$ vapor is the rhombohedron. Thus, presumably,

$$\gamma_{ch,(10\bar{1}1)} < \gamma_{ch,(0001)}.$$

Now, provided $\gamma_{ch,(10\bar{1}0)}$ is sufficiently large to overshadow the fact that at temperatures below 600 °C,

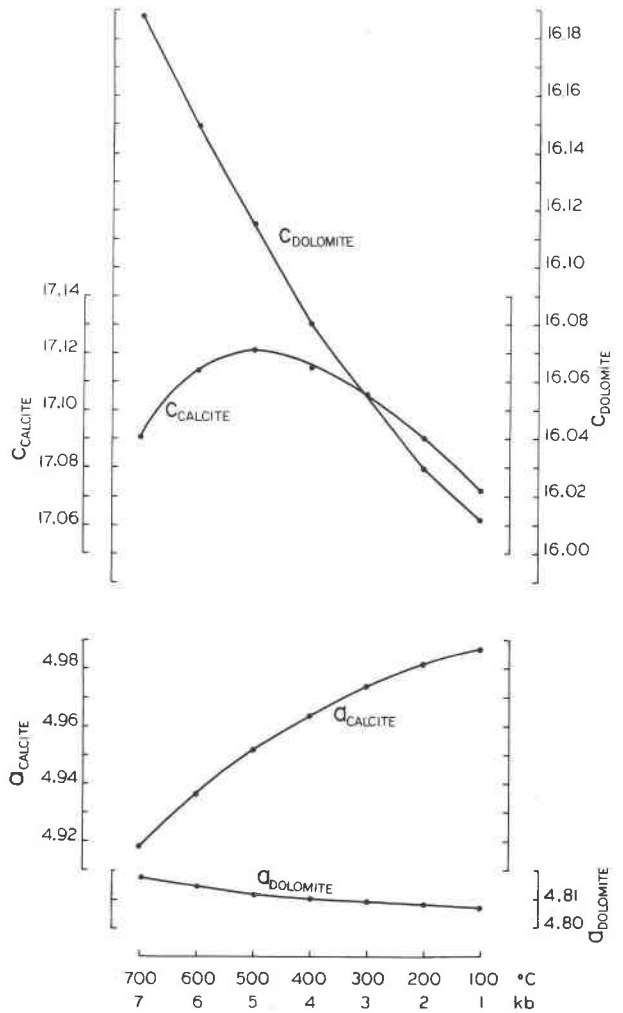$$\gamma_{st,(0001)} \approx \gamma_{st,(10\bar{1}0)}$$

Fig. 6. Calculated cell dimensions (a, c) of magnesian calcite and dolomite at the combinations of temperature (°C) and pressure (kbar) indicated on the horizontal axis (data from Table 2).

(Table 3), and if $\gamma_{ch} - \gamma_{st}$ for (10$\bar{1}$1) and (0001) are numerically comparable, then

$$\gamma_{(10\bar{1}1)} \approx \gamma_{(0001)},$$

and the equilibrium shape of a dolomite particle embedded in calcite is a body bounded by both (10$\bar{1}$1) and (0001) planes.

Some of the observed dolomite plates (Fig. 4) may be viewed as truncated rhombohedra in which (0001) planes are relatively large. If these represent the equilibrium shape, then the relative dimensions of the plates (width to thickness ratio) should be constant, regardless of size (Kretz, 1966). This ratio does vary, however, as shown especially in Figure 4f. Alternatively the equilibrium shape may be represented by the small, near-equidimensional truncated rhombohedron shown in Figure 4o.

TABLE 3.   Calculated Misfit and dislocation density on magnesian calcite–dolomite interface planes

T (°C)	P (kbar)	Misfit (δ) as %			No. of dislocations/cm² on interface planes (×10⁻¹¹)		
		along **a**	along **c**	along ε	(0001)	(10$\bar{1}$0)	(10$\bar{1}$1)
700	7	2.1	5.6	2.8	2.1	2.8	2.9
600	6	2.5	6.0	3.2	3.0	3.6	4.1
500	5	2.9	6.2	3.6	4.0	4.3	5.2
400	4	3.2	6.4	3.8	4.7	4.8	6.0
300	3	3.4	6.5	4.0	5.5	5.3	6.8
200	2	3.6	6.6	4.2	6.1	5.6	7.5
100	1	3.7	6.6	4.3	6.5	5.8	7.9

*Note: a, c, ε = lines parallel to **a**, **c**, and edge of rhombohedral plane, respectively. δ = ($d_{calcite}$ − $d_{dolomite}$)/$d_{dolomite}$, where d is cation (Ca,Mg) spacing along **a**, **c**, or ε.*

VOLUME CHANGE

A contribution to strain not considered above results from the difference in volume between a microcrystal produced by exsolution and the space available to it within the host (Nabarro, 1940). This could be a factor in the growth of plate or rodlike particles rather than equidimensional particles of smaller interfacial area.

The cell-dimension data of Table 2 were combined with the coefficients and mole fractions of Equation 3 to obtain estimates of decremental changes in volume for the exsolution reaction. This calculation assumes that the volume of mixing of dolomite and calcite components in magnesian calcite is negligible, for which evidence was provided by Mackenzie et al. (1983). The volume change was found to be −0.04% for each of the three 100 °C decrements from 600 to 300 °C.

Although the overall volume change is very small, the expansion of a (calcite) upon cooling could possibly play a role in determining the shape and orientation of exsolved dolomite particles. Consider, for example, a spherical volume of homogeneous magnesian calcite at 600 °C, 6 kbar, which cools to 500 °C, 5 kbar, with the release of 6.2 vol% dolomite. The data of Table 1 may be used to show that the mean c dimension of magnesian calcite is thereby increased by a small factor of 1.0004, whereas mean a is increased by a much larger factor of 1.003. Superimposed on this is an overall decrease in calcite volume by a factor of 0.938. Thus, the spherical volume would be least distorted if the separated dolomite occurred as plates or lamellae and if these lay normal to c (as observed), rather than normal to **a**. Similar conclusions hold for a change from 500 °C, 5 kbar to 400 °C, 4 kbar. Further study is needed to evaluate this effect.

NUCLEATION, GROWTH, DIFFUSION

Goldsmith (1960) proposed that oriented plates and rods of dolomite in calcite were produced by a solid-state exsolution process, but he expressed reservation concerning exsolution at low temperatures and suggested that phase separation below 400–500 °C may occur by an aqueous solution-reprecipitation mechanism. Grover and Kubanek (1983 and pers. comm.) suggested that solution-reprecipitation is the *dominant* process of phase separation wherever fluids are present.

With reference to the present study area, H_2O was obviously introduced locally to produce tremolite from diopside and serpentine from forsterite, but it is debatable whether the H_2O existed as a discrete fluid phase or as molecules dispersed along grain boundaries (Kretz, 1980). Even if a discrete fluid was present, it seems unlikely that dolomite precipitated from this fluid would crystallize as oriented plates and rods, as shown in Figure 4, and that calcite precipitated from the fluid would contain concentration gradients, as shown in Figure 5. It is assumed therefore that the separation of dolomite from magnesian calcite in the study specimens occurred by way of an exsolution process, and the mechanisms involved will now be considered.

Consider a volume of calcite-dolomite marble at 700 °C, 7 kbar, and suppose that the volume begins to cool at about 3 °C/m.y. to a point below the solvus. According to the classical theory of homogeneous nucleation, the Gibbs energy of a small particle (an embryo) of dolomite produced in homogeneous calcite is

$$\Delta G = V(-\Delta G_V + \Delta G_S) + \Sigma \gamma_i A_i,$$

where ΔG_V and ΔG_S are the Gibbs energy change and the strain energy per unit volume of dolomite produced, V is the volume of the embryo, and γ_i and A_i are the specific interfacial energy and the area of interface i. At small particle size (radius r < critical radius r^*), the last term dominates, and the embryo is unstable; however, fluctuations permit occasional growth to radius r^*, beyond which $V\Delta G_V$ is dominant and the particles increase in size spontaneously. At the critical point, i.e., when the embryo becomes a nucleus of radius r^*,

$$r^* = 2\gamma/(\Delta G_V - \Delta G_S)$$
$$\Delta G^* = 16\pi\gamma^3/[3(\Delta G_V - \Delta G_S)^2].$$

These equations assume a near-spherical polyhedron of constant interfacial energy (γ). They express the decrease in r^* brought about by an increase in ΔG_V, i.e., by a decrease in temperature. More important, the equations show that a small decrease in γ may give rise to a large decrease in ΔG^*.

Applying these considerations to the nucleation of dolomite in general (including heterogeneous nucleation), it is evident that the following sequence of nucleation sites represents increasing values of ΔG^* for given values of ΔG_V and ΔG_S: calcite-dolomite grain boundaries < calcite-calcite grain boundaries < twin planes < dislocations < random homogeneous sites in calcite. Crystallization at an existing calcite-dolomite grain boundary does not require a nucleation event, crystallization at calcite-calcite grain and twin boundaries reduces $\Sigma \gamma A$ to the extent that some interface is consumed, and crystallization on dislocations reduces ΔG^* by the amount of the dislocation energy.

Twin lamellae are common in the calcite crystals of the

present study, but it was not possible to establish that twin planes formed nucleation sites for dolomite. Etch pits in calcite similar to those described by Braillon et al. (1974, Fig. 5) were locally observed, and dislocations probably provided some nucleation sites. Homogeneous nucleation in metals is rare (Porter and Easterling, 1981), but in magnesian calcite, the random distribution of many Ca and Mg atoms will inherently produce a relatively few clusters of atoms approximately a dolomite configuration, and homogeneous nucleation may be possible.

It is evident from Figure 4 that a bimodal particle-size distribution exists at many places (e.g., Figs. 4c, 4d, 4f, 4g, 4h, 4i), and if some external grains of dolomite were also produced by exsolution, as discussed above, the size distribution is trimodal. This observation suggests that nucleation may have occurred in three stages, as follows. During an early, high-temperature stage (1) exsolved Mg diffused to grain boundaries, where it was deposited on primary dolomite or nucleated and grew at calcite-calcite boundaries. During an intermediate, moderate-temperature stage (2), dolomite nucleated within calcite crystals to produce oriented plates and rods, such as those shown in Figures 4d, 4e, 4j, 4k, and 4n. These microcrystals are somewhat variable in size (Fig. 4j), suggesting that nucleation was not instantaneous. A random spatial distribution of microcrystals (Fig. 4j) is consistent with homogeneous nucleation or the presence of a high density of imperfections or other favorable nucleation sites. Nucleation of rods at grain centers, followed by radial growth toward the margins (Fig. 4b) may have resulted from gradients in concentration of Mg produced during state 1. A later, low-temperature stage (3) was characterized by the massive precipitation of small particles such as those shown in Figures 4i, 4o, and 4p. Crystallization was erratic, but where very small particles are abundantly present, they are noticeably less abundant in the Mg-depleted regions near rods (Fig. 4g), thereby presenting evidence that the fine particles postdate the rods of stage 2. Where isolated small particles were produced (Fig. 4o), the nucleation rate obviously reached a maximum, but where an interconnected network was produced (Fig. 4i), the nucleation density cannot be determined. Restricted diffusion during stage 3 may be partially responsible for precipitation of many closely spaced particles.

Behavior similar to that proposed above is found in some metal systems. In the Fe-C system, for example, the precipitation of ferrite exsolved from austenite on controlled cooling occurs first on grain boundaries, then as plates that grow from grain boundaries, and finally as microcrystals within grains of austenite (Shewmon, 1969).

The tabular morphology of dolomite microcrystals can be understood by assuming that the nuclei possessed the shape of a truncated rhombohedron (as discussed above) and by supposing that the $(10\bar{1}1)$ interfaces advanced more rapidly than the (0001) interfaces (Fig. 7). The result is a plate with rhombohedral terminations similar to those observed in Figure 4f. The calculated higher dislocation density on $(10\bar{1}1)$ compared with (0001) (Table 3) is con-
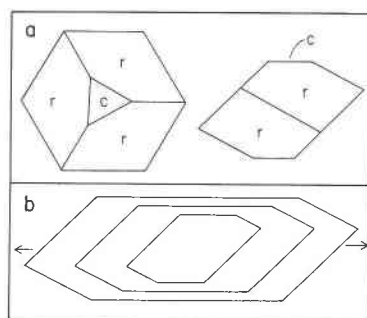

Fig. 7. (a) Plan and elevation of a truncated rhombohedron. (b) Growth of a plate (cross section) by rapid advance of rhombohedral interfaces and slow advance of basal interfaces (schematic).

sistent with the generalization that least coherent interfaces advance most rapidly (Porter and Easterling, 1981). This interpretation rests on the knowledge that relative rates of advance of different interfaces of an inclusion need not be governed entirely by their interfacial energies, and it implies that dolomite plates represent distorted equilibrium shapes.

The growth of segmented rods, such as those shown in Figure 4k, may have occurred by a "budding" process. Beginning with a rhombohedron that has grown to a mean dimension of about 10 μm, continued growth evidently occurred by the "nucleation" of a new rhombohedron at one of the six side corners of the existing rhombohedron (Fig. 8). Development of the rods thus occurred by the propagation of rhombohedra, followed by some growth everywhere on the rods to cause rounding of corners. The cause for this behavior is not known, but an analogy with dendritic growth is obvious.

Nonsegmented rods, such as those shown in Figures 4c, 4d, and 4e, are apparently bounded by incoherent interfaces, but the tendency for these to lie within $(10\bar{1}1)$ and parallel to **a** (the long diagonal) may be attributed to slow growth of partially coherent interfaces lying subparallel to $(10\bar{1}1)$, relative to incoherent terminal interfaces (top left corner of Fig. 4c) lying at a large angle to $(10\bar{1}1)$.

The above interpretation requires a displacement of Ca and Mg atoms in magnesian calcite, brought about by Ca-Mg exchange diffusion. The displacement required ranges from a few millimeters during stage 1 to a few tens of micrometers during stage 2, to a few micrometers or less during stage 3, corresponding to a temperature drop extending from 600–700 °C to possibly 100–200 °C. In the absence of experimental data on Ca-Mg exchange diffusion in calcite, a proposal for the diffusion equation may be expressed as follows:

$$D = (9.0 \times 10^{-7})10^{-6.9 \times 10/RT}, \qquad (5)$$

i.e., $D_0 = 9.0 \times 10^{-7}$ cm²·s⁻¹ and $Q = 6.9 \times 10$ kJ· mol⁻¹.

At 600, 400, and 200 °C (the estimated temperatures for stages 1, 2, and 3, respectively), Equation 5 produces
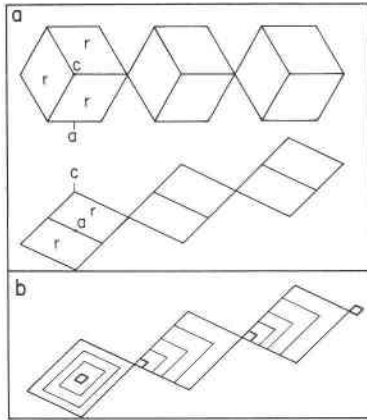
Fig. 8. (a) Plan (top) and elevation of three connected rhombohedra. (b) Growth of a segmented rod (cross section) by the propagation of rhombohedra (schematic).

mean displacements [$\bar{x} = (Dt)^{1/2}$] of 10, 0.39, and 0.001 mm for durations of 100 m.y. Equation 5 is in agreement with the conclusion of Bratter et al. (1972) (D for Ca self-diffusion in calcite at 800 °C is less than 5×10^{-16} cm²·s⁻¹) only if D for exchange diffusion is greater than D for self-diffusion by a factor of about 100.

CONCLUSIONS

The scanning electron microscope has revealed an astonishing diversity in the size, shape, orientation, and distribution of dolomite microcrystals embedded in calcite from high-grade Grenville marble. Most conspicuous are plates with rhombohedral terminations oriented normal to c of calcite, parallel segmented rods, and very small rhombohedra, some of which are truncated by (0001). Most of these particles are crystallographically coaxial with the enclosing calcite.

All of the microcrystals evidently separated from magnesian calcite during cooling from peak metamorphic conditions of about 700 °C and 7 kbar, at a cooling rate of a few degrees per million years.

Mg-depleted zones about dolomite plates and rods are viewed as stranded diffusion depressions and are presented as evidence of dolomite separation by a diffusion-controlled exsolution process. During exsolution, Fe was sequestered by dolomite and Sr by calcite to produce dolomite/calcite distribution coefficients of 5.0 and 0.5, respectively.

An analysis of (0001) and (10$\bar{1}$1) interface planes between coaxial dolomite and calcite leads to the conclusion that the structural component of interfacial energy is less on (0001) (lower dislocation density) and the chemical component of interfacial energy is less on (10$\bar{1}$1), giving nearly equal values of total specific interfacial energy for both. This implies that the equilibrium shape of a dolomite particle embedded in calcite is a truncated rhombohedron, possibly one of near-equidimensional shape as observed locally.

Volume considerations lead to the conclusion that al-though the overall volume change for the exsolution reaction is very small, the anisotropic and anomalous thermal expansion of calcite results in a minimum of volume distortion if the exsolved dolomite occurs as lamellae or plates and if they are oriented normal to c of calcite. Additional data are needed to determine whether this volume distortion is an important consideration.

The microstructures raise numerous questions regarding the nucleation and growth of dolomite and the rate of cation diffusion in calcite. Three successive stages in the exsolution of dolomite are postulated, representing a progressive increase in nucleation rate and a decrease in Ca-Mg diffusion rate with falling temperature. These are (1) exsolution of dolomite to grain boundaries, (2) nucleation within calcite and subsequent growth to form plates and rods, and (3) massive precipitation of very small particles. During stage 2, plates were produced from truncated rhombohedra by rapid advance of rhombohedral interfaces and slow advance of basal interfaces, and rods were produced by the propagation of rhombohedra from one of the six side corners of the preceding rhombohedron.

Obviously, much more thought and study are needed before all of the complex microstructures shown in Figure 4 will be fully understood.

REFERENCES CITED

Agrell, S.O., Long, J.V.P., and Ogilvie, R.E. (1963) Nickel content of kamacite near the interface with taenite in iron meteorites. Nature, 198, 749–750.

Althoff, P.L. (1977) Structural refinements of dolomite and magnesian calcite and implications for dolomite formation in the marine environment. American Mineralogist, 62, 772–783.

Berger, G.W., and York, D. (1981) ⁴⁰Ar/³⁹Ar dating of the Thanet gabbro, Ontario: Looking through the Grenvillian metamorphic veil and implications for paleomagnetism. Canadian Journal of Earth Sciences, 18, 266–273.

Birch, F. (1966) Compressibility; elastic constants. In S.P. Clark, Jr., Ed., Handbook of physical constants. Geological Society of America Memoir 97, 97–173.

Bischoff, W.D., Bishop, F.C., and Mackenzie, F.T. (1983) Biogenically produced magnesian calcite: Inhomogeneities in chemical and physical properties; comparison with synthetic phases. American Mineralogist, 68, 1183–1188.

Bollmann, W. (1970) Crystal defects and crystalline interfaces. Springer-Verlag. Berlin.

Bollmann, W., and Nissen, H.-U. (1968) A study of optimal phase boundaries: The case of exsolved alkali feldspars. Acta Crystallographica, A 24, 546–557.

Braillon, P., Mugnier, J., and Serughetti, J. (1974) Transmission electron microscope observations of the dislocations in calcite single crystals. Crystal Lattice Defects, 5, 73–78.

Bratter, P., Möller, P., and Rösick, U. (1972) On the equilibrium of co-existing sedimentary carbonates. Earth and Planetary Science Letters 14, 50–54.

Carpenter, A.B. (1967) Mineralogy and petrology of system CaO-MgO-CO$_2$-H$_2$O at Crestmore, California. American Mineralogist, 52, 1341–1363.

Coomaraswamy, A.K. (1902) The crystalline limestones of Ceylon. Quarterly Journal of the Geological Society, 58, 399–424.

Crank, J. (1975) The mathematics of diffusion. Clarendon Press, Oxford.

Easton, R.M. (1986) Geochronology of the Grenville province. In J.M. Moore, A. Davidson, and A.J. Baer, Eds., The Grenville province. Geological Association of Canada Special Paper 31, 127–174.

Evans, R.C. (1966) An introduction to crystal chemistry. Cambridge University Press, Cambridge.

Fleet, M.E. (1982) Orientation of phase and domain boundaries in crystalline solids. American Mineralogist, 67, 926–936.

Garde, A.A. (1977) Calcite-dolomite thermometry: Negative evidence from the Marmorilik formation, West Greenland. Contributions to Mineralogy and Petrology, 62, 265–270.

Gittins, J. (1979) Problems inherent in the application of calcite-dolomite geothermometry to carbonatites. Contributions to Mineralogy and Petrology 69, 1–4.

Goldsmith, J.R. (1960) Exsolution of dolomite from calcite. Journal of Geology, 68, 103–109.

Goldsmith, J.R., and Heard, H.C. (1961) Subsolidus phase relations in the system CaCO$_3$-MgCO$_3$. Journal of Geology, 69, 45–74.

Goldsmith, J.R., and Newton, R.C. (1969) P-T-X relations in the system CaCO$_3$-MgCO$_3$ at high temperatures and pressures. American Journal of Science, 267A, 160–190.

Goldsmith, J.R., Graf, D.L., and Joensuu, O.I. (1955) The occurrence of magnesian calcites in nature. Geochimica et Cosmochimica Acta, 7, 219–230.

Graf, D.L., and Goldsmith, J.R. (1955) Dolomite-magnesian calcite relations at elevated temperatures and CO$_2$ pressures. Geochimica et Cosmochimica Acta, 7, 109–128.

Grover, J., and Kubanek, F. (1983) The formation of ordered dolomite from high-magnesian calcite at 250° to 350 °C and 1500 bars: Epitactic growth with optimal phase orientation, and implications for carbonate diagenesis. American Journal of Science, 283A, 514–539.

Harker, R.I., and Tuttle, O.F. (1955) Studies in the system CaO-MgO-CO$_2$. Part 2. Limits of solid solution along the binary join CaCO$_3$-MgCO$_3$. American Journal of Science, 253, 274–282.

Hoel, P.G. (1964) Introduction to mathematical statistics. Wiley, New York.

Ioffe, L.I., Krylov, I.N., and Nikitina, L.P. (1973) Magnesian calcites as indicators of temperature of metamorphism (exemplified by the Archean complex in Baykal region). International Geological Review, 15, 416–427.

Joplin, G.A. (1935) The exogenous contact zone at Ben Bullen, New South Wales. Geological Magazine, 72, 385–400.

Kretz, R. (1966) Interpretation of the shape of mineral grains in metamorphic rocks. Journal of Petrology, 7, 68–94.

——— (1969) On the spatial distribution of crystals in rocks. Lithos, 2, 38–65.

——— (1980) Occurrence, mineral chemistry, and metamorphism of Precambrian carbonate rocks in a portion of the Grenville province. Journal of Petrology, 21, 573–620.

Long, J.V.P., and Agrell, S.O. (1965) The cathodo-luminescence of minerals in thin section. Mineralogical Magazine, 34, 318–326.

Lorimer, G.W., and Champness, P.E. (1973) Combined electron microscopy and analysis of an orthopyroxene. American Mineralogist, 58, 243–248.

Mackenzie, F.T., Bischoff, W.D., Bishop, F.C., Loijens, M., Schoonmaker, J., and Wollast, R. (1983) Magnesian calcites: Low-temperature occurrence, solubility and solid-solution behavior. Mineralogical Society of America Reviews in Mineralogy, 11, 97–144.

Markgraf, S.A., and Reeder, R.J. (1985) High-temperature structure refinements of calcite and magnesite. American Mineralogist, 70, 590–600.

Metz, P. (1976) Experimental investigation of metamorphism of siliceous dolomites: III. Equilibrium data for the reaction 1 tremolite + 11 dolomite = 8 forsterite + 13 calcite + 9 CO$_2$ + H$_2$O for the total pressures of 3000 and 5000 bars. Contributions to Mineralogy and Petrology, 58, 137–148.

Nabarro, R.F.N. (1940) The influence of elastic strain on the shape of particles segregating in an alloy. Proceedings of the Physical Society, 52, 90–93.

Nesbitt, B.E., and Essene, E.J. (1982) Metamorphic thermometry and barometry in a portion of the southern Blue Ridge province. American Journal of Science, 282, 701–729.

Perkins, D., III, Essene, E.J., and Marcotty, L.-A. (1982) Thermometry and barometry of some amphibolite-granulite facies rocks from the Otter Lake area, southern Quebec. Canadian Journal of Earth Sciences, 19, 1759–1774.

Porter, D.A., and Easterling, K.E. (1981) Phase transformations in metals and alloys. Van Nostrand Reinhold, New York.

Puhan, D. (1984) Microtexture of dolomite within exsolved magnesian calcite—Examples from the Damara orogen (Namibia). Contributions to Mineralogy and Petrology, 87, 98–99.

Puustinen, K. (1974) Dolomite exsolution textures in calcite from the Siilinjärvi carbonatite complex, Finland. Bulletin of the Geological Society of Finland, 46, 151–159.

Reeder, R.J. (1983) Crystal chemistry of the rhombohedral carbonates. Mineralogical Society of America Reviews in Mineralogy, 11, 1–47.

Reeder, R.J., and Markgraf, S.A. (1986) High-temperature crystal chemistry of dolomite. American Mineralogist, 71, 795–804.

Rice, J.M. (1977) Contact metamorphism of impure dolomitic limestone in the Boulder aureole, Montana. Contributions to Mineralogy and Petrology, 59, 237–259.

Robinson, P., Ross, M., Nord, G.L., Smyth, J.R., and Jaffe, H.W. (1977) Exsolution lamellae in augite and pigeonite: Fossil indicators of lattice parameters at high temperature and pressure. American Mineralogist, 62, 857–873.

Sheppard, S.M.F., and Schwarcz, H.P. (1970) Fractionation of carbon and oxygen isotopes and magnesium between coexisting metamorphic calcite and dolomite. Contributions to Mineralogy and Petrology, 26, 161–198.

Shewmon, P.G. (1969) Transformations in metals. McGraw-Hill, New York.

Skippen, G. (1974) An experimental model for low pressure metamorphism of siliceous dolomite marble. American Journal of Science, 274, 487–509.

Stranski, I.N. (1949) Forms of equilibrium of crystals. Discussions of the Faraday Society, 5, 13–21.

Willaime, C., and Brown, W.L. (1974) A coherent elastic model for the determination of the orientation of exsolution boundaries: Applications to the feldspars. Acta Crystallographica, A 30, 316–331.

Wilson, A.E. (1964) Geology of the Ottawa–St. Lawrence lowland, Ontario and Quebec. Geological Survey of Canada Memoir 241.